training set size reflects the true priors. The classification maps for LOOC+DAFE+ECHO and bLOOC+DAFE+ECHO are shown in Figs. 4 and 5, respectively.

VI. Conclusion

The inverse of a covariance matrix becomes ill or poorly posed if the training set size is small compared to the dimensionality. Conventionally, the stabilization of the covariance estimate has been accomplished by regularization, which tends to reduce the variance of the estimate at the expense of increased bias. This method can also be viewed as a compromise between the linear and quadratic classifiers. In this paper, a regularization method under the Bayesian setting has been proposed. The proposed bLOOC estimation method was shown to have better performance than other methods when the training set size reflects the true priors of the classes. This is particularly true for remote-sensing applications since more training samples are usually selected for larger classes. When used in conjunction with DAFE, the proposed covariance estimation was demonstrated to circumvent the limited training set size problem. However, since the leave-one-out likelihood is used as the criterion for the estimator, it has the drawback of not being directly related to class separability and, subsequently, the classification accuracy. Therefore, some smooth loss function derived from the class separability is recommended for future work. Also, since DAFE does not work well when the classes have similar mean values, alternative feature extraction or classification methods need to be explored.

References

[1] S. P. Lin and M. D. Perlman, "A Monte Carlo comparison of four estimators of a covariance matrix," in *Multivariate Anal.—VI: Proc. 6th Int. Symp. Multivariate Anal.*, P. R. Krishnaiah, Ed. Amsterdam, The Netherlands: Elsevier, 1985, pp. 411–429.

[2] P. W. Wahl and R. A. Kronmall, "Discriminant functions when covariances are equal and sample sizes are moderate," *Biometrics*, vol. 33, pp. 479–484, 1977.

[3] J. F. Friedman, "Regularized discriminant analysis," *J. R. Stat. Soc.*, vol. 84, pp. 17–42, 1989.

[4] J. P. Hoffbeck and D. A. Landgrebe, "Covariance matrix estimation and classification with limited training data," *IEEE Trans. Pattern Anal. Machine Intell.*, vol. 18, pp. 763–767, July 1996.

[5] W. Rayens and T. Greene, "Covariance pooling and stabilization for classification," *Computat. Stat. Data Anal.*, vol. 11 pp. 17–42, 1991.

[6] S. Tadjudin, "Classification of high dimensional data with limited training samples," Ph.D. dissertation, Sch. Elect. Comput. Eng., Purdue Univ., West Lafayette, IN, 1998. Available from http://dynamo.ecn.purdue.edu/~landgreb/publications.html.

[7] C. Lee and D. A. Landgrebe, "Feature extraction based on decision boundaries," *IEEE Trans. Pattern Anal. Machine Intell.*, vol. 15, pp. 388–400, Mar. 1993.

[8] K. Fukunaga, *Introduction to Statistical Pattern Recognition*, 2nd ed. Boston, MA: Academic, 1990.

[9] R. L. Kettig and D. A. Landgrebe, "Classification of multispectral image data by extraction and classification of homogeneous objects," *IEEE Trans. Geosci. Electron.*, vol. GE-14, pp. 19–26, Jan. 1976.

SAR Interferometry on a Very Long Time Scale: A Study of the Interferometric Characteristics of Man-Made Features

Stefania Usai and Roland Klees

***Abstract*— Anthropogenic features show up as highly coherent objects even in heavily decorrelated interferograms. In order to assess whether the information from such features is still usable, the stability of their phase and coherence is analyzed through a series of interferograms. The results indicate that these features can remain interferometrically stable over several years.**

***Index Terms*— Coherence, differential SAR interferometry, man-made features.**

I. Introduction

Synthetic aperture radar (SAR) interferometry has turned out to be a very powerful technique for the measurement of land deformations, but it requires the observed area to be correlated, which can restrict its applicability to small time scales. The result is that deformation processes that would require monitoring by means of interferometric SAR (INSAR) at long time scales seems to be outside of the capabilities of this technique.

It has been observed, however, in almost totally decorrelated interferograms, that some features, mainly of anthropogenic nature, maintain high coherence even over time scales of years. The question arises whether this remaining information can still be used to assess terrain deformations by means of the differential technique. If this is possible, the decorrelation problem could be bypassed, resulting in the extension of the range of possible applications of INSAR.

The aim of this paper is to study the interferometric characteristics of highly coherent features to assess how much interferometric information they contain and whether this information can be used for the study of slow deformation processes. For this purpose, a time series of interferograms of a test area in The Netherlands has been processed; the details and some remarks about the construction of the series are given in Section II. A sample of features showing high coherence on a long time scale has been selected, and their coherence has been studied over the whole series. The results of this analysis are presented in Section III. For a subset of these features, the phase stability has also been checked by means of the differential technique. The procedure applied and the results obtained are discussed in Sections IV and V. Finally, some remarks and conclusions are given in Section VI.

II. 1992–1996 Time Series

The test site for this study is the area around the city of Groningen, in the northern part of The Netherlands. The area is well known for its land subsidence, caused by the extraction of natural gas: the rate of land subsidence amounts to a maximum of 1 cm/yr.

The set of images to be used for the construction of the time series has been selected on the basis of the following criteria.

- Same single-look complex (SLC) image has to be used as master for all interferometric pairs. In this way, a given pixel represents the same area in all interferograms.

Manuscript received April 16, 1998; revised July 29, 1998.

The authors are with the Delft Institute for Earth Oriented Space Research (DEOS), Faculty of Civil Engineering and Geosciences, Delft University of Technology, 2629JA Delft, The Netherlands (e-mail: usai@geo.tudelft.nl).

Publisher Item Identifier S 0196-2892(99)04336-3.

TABLE I
GRONINGEN DATA SET. THE FIFTH COLUMN SHOWS THE TIME SPAN IN DAYS, THE SIXTH THE SERIAL NUMBER OF THE INTERFEROGRAM

master	slave	B_{par}	B_{perp}	days	no
16-3-96	17-3-96	-17	24	1	9
16-3-96	11-2-96	36	212	34	8
16-3-96	20-4-96	50	145	35	7
16-3-96	21-4-96	18	79	36	6
16-3-96	6-1-96	-109	-129	70	5
16-3-96	20-8-95	-62	-272	209	4
16-3-96	19-8-95	-26	-190	210	3
16-3-96	15-10-92	5	25	1248	2
16-3-96	10-9-92	43	52	1283	1

- Only the interferometric pairs having a perpendicular component of the baseline $B_\perp$ less than 300 m are considered. We observed that, in general, interferograms with baselines longer than 300 m are heavily affected by baseline decorrelation.
- Since we want to apply the differential technique, it should be possible to obtain a (well-correlated) interferogram on one or 35 days with a sufficiently large baseline to be used as the reference interferogram.
- On long time scales, very short perpendicular baselines are required to apply the differential technique.

By means of these criteria, the images were selected and nine interferograms were generated, whose characteristics are given in Table I. The last column contains the interferogram serial numbers, which will be used from now on to refer to the interferograms.

Further characteristics of the time series are as follows.

- Azimuth filtering has been applied. Tests confirmed what was already highlighted in the literature [1], [4], i.e., that azimuth filtering highly improves the coherence. This is particularly important for the long time scale interferograms, in which the coregistration is more difficult because of the low coherence. In some cases, coregistration did not succeed without azimuth filtering.
- Coherence was estimated over a 2 × 10 window. This seemed a good trade-off between the necessities 1) of choosing a large enough window to give a reliable estimate of the coherence and 2) of working on the highest possible resolution, since anthropogenic features are usually very small compared to the spatial scale of the image.
- Final products, i.e., the coherence and phase images, are averaged over 2 × 10 pixels. The fact that the coherence estimation window and the multilook size are the same allows us to refer directly to the estimated coherence to the corresponding phase value in the same pixel. In other words, each multilooked pixel has a value in coherence and phase that is the average of the same original pixels used for estimating the coherence. Note that this does not imply that neighboring multilooked pixels are uncorrelated. In fact, multilooking uses an averaging window, while the coherence estimation is performed with a shifting window: therefore, the single-look pixels at the border of two adjacent multilooking windows, which will contribute to two different average values, share actually a portion of the estimation window. The choice of a multilooking window equal in size to the estimation window, however, reduces the statistical correlation only to the adjacent multilooked pixels.

III. ANALYSIS OF THE COHERENCE

Fig. 1 shows the coherence images on the shortest (one day, ERS tandem pair 9) and on the longest (about 3 1/2 yr, ERS1/ERS1 pair 1) time interval considered here. Only those pixels having coherence higher than 0.8 in the coherence image 1 have been taken into account. We focused in particular on the area of the city of Assen (low left in Fig. 1), which has an extension of 200 × 300 pixels and contains a sufficiently large number of high-coherence pixels to be analyzed statistically. The coherence of the selected pixels that are located in this area has thus been traced in the whole time series. Fig. 2 represents the coherence of the selected points for all interferograms: each column represents an interferogram of the series, each horizontal line contains the values of the coherence for a given point. It is evident from Fig. 2 that interferogram 8 presents a significantly lower coherence for the same features than all other interferograms, suggesting that some factors have affected its quality. Indeed, the slave image has been acquired in February, in a period of frequent snowfalls, and it is likely that the different weather conditions in February and in March, when the master has been acquired, caused the decorrelation. Another source of decorrelation could be the relatively long perpendicular baseline (212 m).

In general, Fig. 2 does not indicate any trend of coherence over time. Features showing high coherence in the longest time span interferogram (1) do not necessarily show high values on shorter time spans as well. As we should expect, the different specific conditions (weather, seasonality, satellite configuration) under which the slaves have been acquired may affect the coherence more than the time interval between master and slave.

IV. ANALYSIS OF THE PHASE

The second step of the analysis consisted of checking whether those features showing constantly high coherence over the time series do also maintain phase stability in time. For the test, the differential INSAR technique [5] has been applied. For the analysis of the phase values, the series has been reduced to the six interferograms no. 1, 2, 5, 6, 7, and 9. Interferogram 7, which has $B_\perp = 145$ m, has been chosen as reference interferogram; therefore, interferograms 3 and 4, which have a longer perpendicular baseline, have been excluded.

The sample of high-coherence points is the same as considered for the coherence analysis, namely, the area of Assen. This area is particularly suitable not only because it has a large number of highly coherent features over 3-1/2 yr, but also because it is outside the subsidence area. Any phase variations to be detected by means of the differential technique would therefore mean “instability” of the coherent features with respect to all the other effects than real deformations. Note that, since the area is rather limited in size, it can be assumed that atmospheric effects, if present, are likely to be uniform, so that they should be eliminated when taking spatial differences.

From the set of pixels used for the study of the coherence (126 pixels), only those maintaining coherence above 0.8 in all six interferograms were selected, resulting in a subset of 42 pixels. In each interferogram, the relative phase of each pixel with respect to a reference pixel (which is the same in all interferograms) has been computed. The reference pixel has been chosen as the pixel with the minimum standard deviation of the coherence over the series. For each of the spatial differences, the value in interferogram 7 has been taken as a reference value and rescaled and subtracted from the corresponding phase difference value in all of the other five interferograms by using the formula [5]:

$$\Delta\phi_{\rm flat}(i) - \frac{B_\perp(i)}{B_\perp(7)}\,\Delta\phi_{\rm flat}(7) = \delta\phi(i) \tag{1}$$

where $\Delta\phi_{\rm flat}(i)$ and $B_\perp(i)$ are the relative phase (earth flattened) of a certain multilooked pixel in interferogram i ($i = 1, 2, 5, 6, 9$) and the perpendicular baseline of interferogram i, respectively. $\Delta\phi_{\rm flat}(7)$

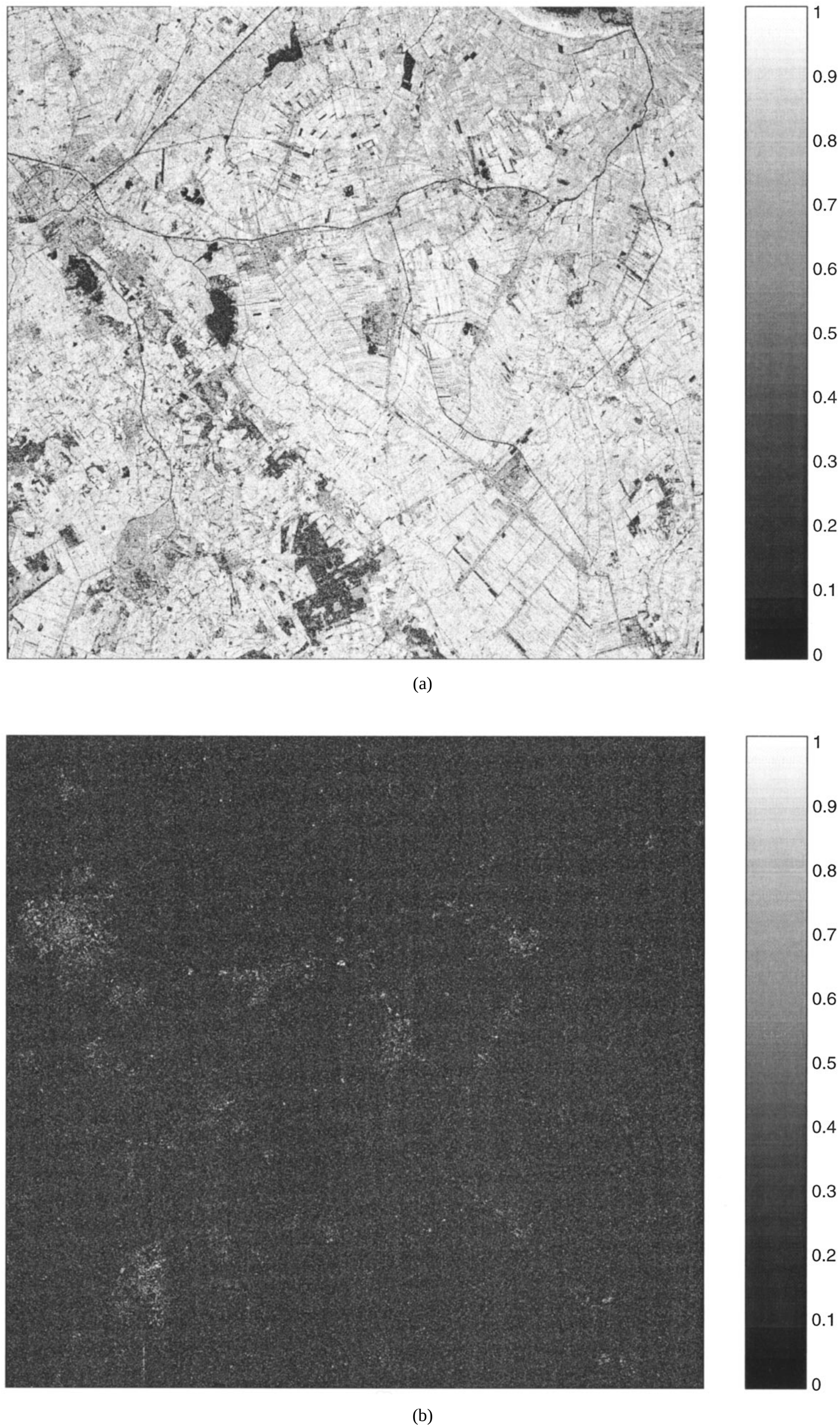

Fig. 1. Coherence images for the time intervals: (a) (16-3-96/17-3-96) and (b) (16-3-96/10-9-92).

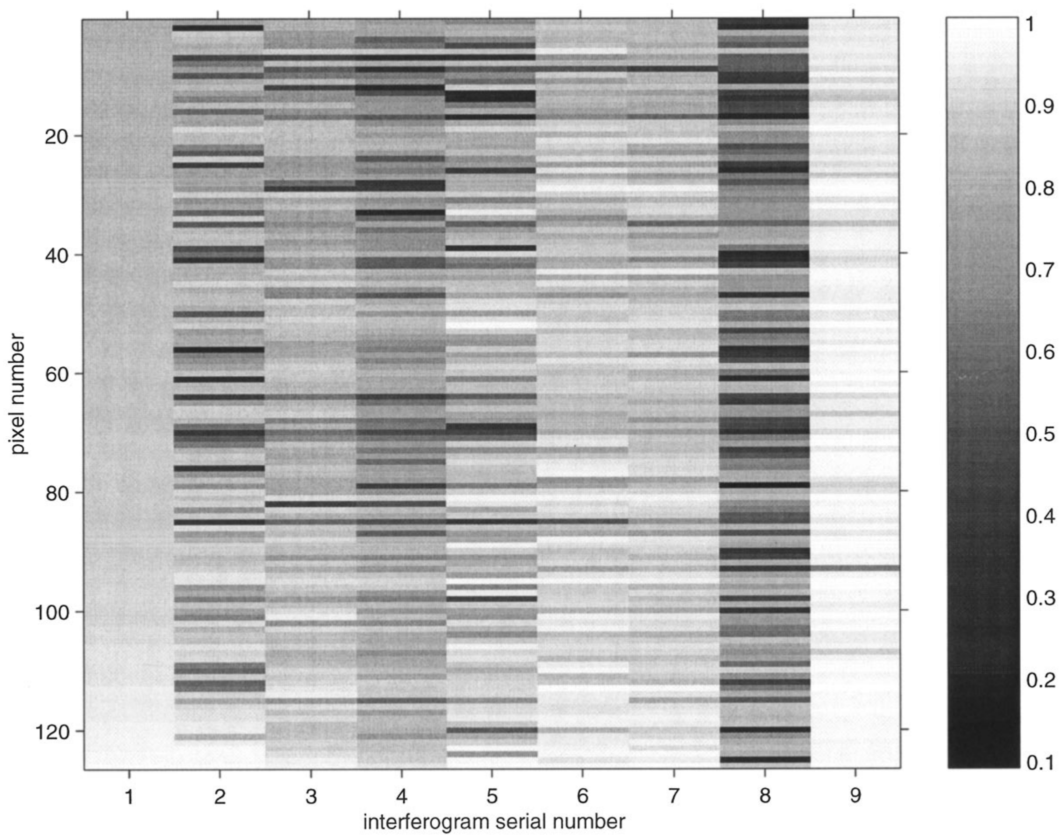

Fig. 2. Coherence values for each multilooked pixel of the "Assen data set" and for each interferogram.

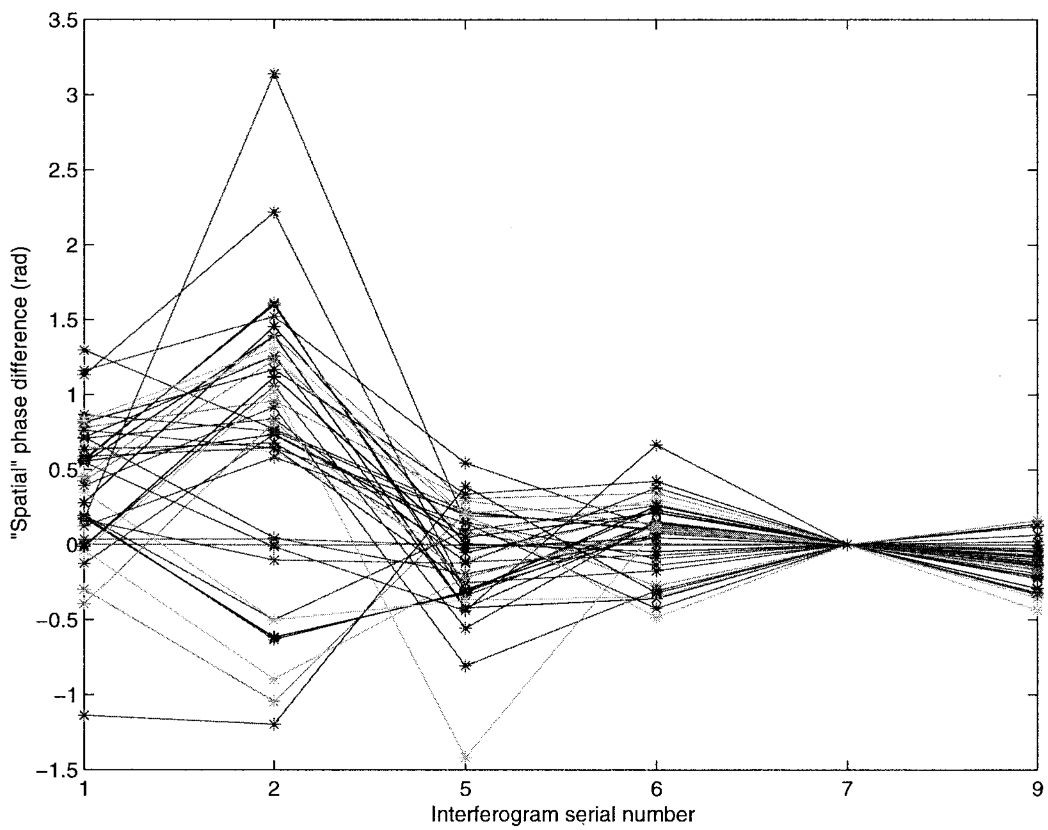

Fig. 3. Differential phase values over the time series for constantly highly coherent pixels (interferogram 7 has zero values because it is taken as reference interferogram).

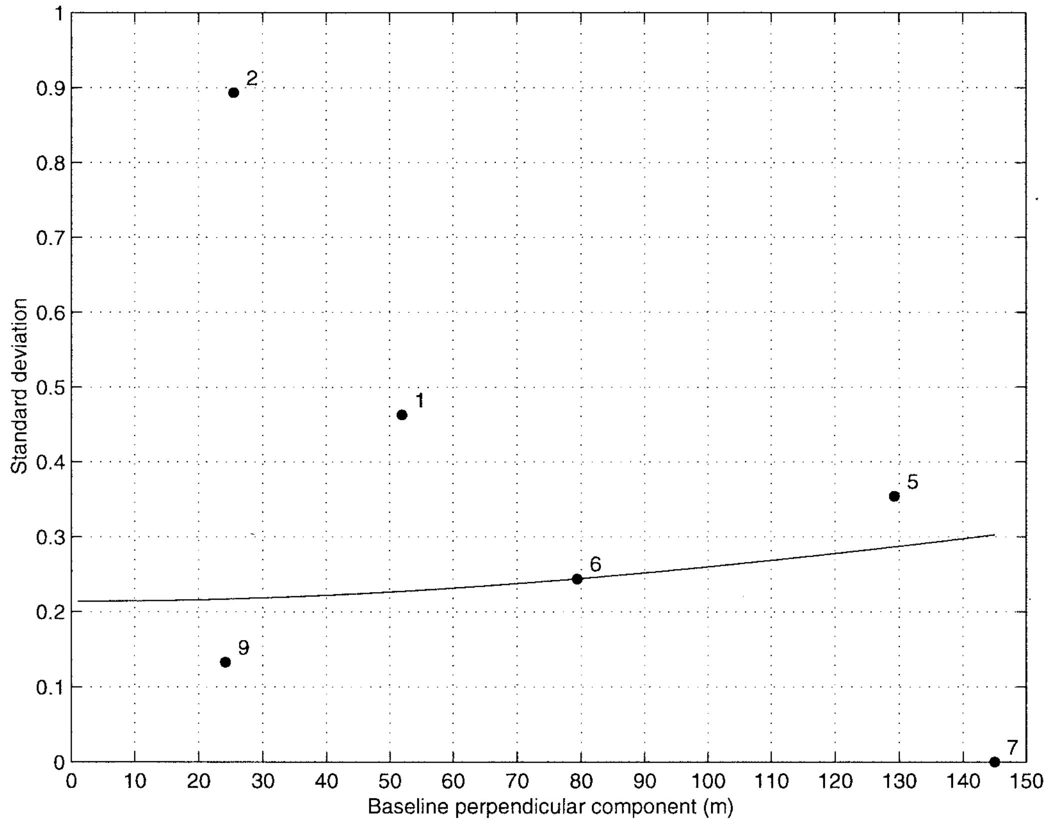

Fig. 4. Standard deviations of the differential phases for each interferogram. The solid line is the "theoretical" standard deviation as derived from the value in interferogram 6, and the • indicates the values computed from the data.

and $B_\perp(7)$ are the same quantities for the reference interferogram, and $\delta\phi(i)$ is the differential phase, which is expected to be zero in absence of subsidence, very small-scale atmospheric effects and noise.

Note that (1) has to be applied to the unwrapped phases. Since the considered area is very flat and due to the short interferometric baselines, however, we can assume that no phase jumps caused by the topography are present. Due to the absence of high buildings in the area, we know, for our baselines, that the "urban" topography cannot cause 2π ambiguities. Hence, we do not need to unwrap the phase, which of course would be necessary if urban and/or natural topography become significant.

The differential phase computed by means of (1) is shown in Fig. 3. Every line is the relative phase difference between one pixel and the reference pixel rescaled according to (1) and plotted along the time series.

From Fig. 3, it seems that most of the pixels considered do maintain phase stability on a long time scale at the level of about one radian. It is also evident that the differential phases in interferogram 2 have undergone some disturbances (perhaps due to meteorological conditions) that have affected the phases of many points. This is also evident from Fig. 4, which shows the standard deviations of all data within an interferogram.

V. First Estimate of the Standard Deviation

The error associated with the determination of the $\delta\phi$ for a certain point P in interferogram i can be computed by simple error propagation applied to (1)

$$\sigma^2(\delta\phi(i)) = \sigma^2(\Delta\phi_{\text{flat}}(i)) + \left(\frac{B_\perp(i)}{B_\perp(7)}\right)^2 \sigma^2(\Delta\phi_{\text{flat}}(7)) \tag{2}$$

where

$$\sigma(\Delta\phi_{\text{flat}}(i)) = \left[\sigma^2(\phi_{\text{flat}}) + \sigma^2(\phi_{\text{flat}}(R))\right]^{1/2} \tag{3}$$

is the standard deviation associated with the spatial phase difference between P and the reference point R in interferogram i. $\sigma(\Delta\phi_{\text{flat}}(7))$ is the same quantity for the reference interferogram, and the $\sigma(\phi_{\text{flat}})$ and $\sigma(\phi_{\text{flat}}(R))$ are the errors associated with the phase values in P and R, respectively. It is not trivial, however, in our case, to estimate the values of $\sigma(\phi_{\text{flat}})$. In fact, the standard deviation for a certain phase value is usually estimated from the corresponding coherence value of the same pixel. The estimator is different though for different kind of scatterers, depending on the type of scatterer considered. So, for extended scatterers, the standard deviation has the expression given by [2]; but for deterministic pointlike scatterers, such as corner reflectors, the phase statistic is quite different, leading to the expression for the standard deviation [3]

$$\sigma = \sqrt{\frac{(1-\gamma)^2}{2 * \gamma^2}} \tag{4}$$

for $|\gamma| \simeq 1$. This formula yields lower values for the standard deviation than the one for extended scatterers [2].

In our case, the nature of the scatterers is not known: reflection may come from a single, very strong, pointlike source, like a corner reflector, but it can also come from several point scatterers or from an homogeneous extended scatterer (where the term "extended" refers to a few tens of pixels in size). Therefore, the choice of the phase probability density function is not straightforward. Moreover, the two formulas mentioned above are given in the case of single-look phase values: in a case like ours, of multilooking, for a rigorous estimate of the standard deviation, we should modify the estimators to take into account the improvement of the estimate due to the averaging.

For these reasons, an empirical approach for the estimation of the standard deviation is preferred to a theoretical approach.

Since interferogram 6 differs from the reference interferogram 7 by only one day, it seems reasonable to assume that for most pixels the area they represent is not changed intrinsically, i.e., that a pixel represents an identical area in 6 and 7. Under this assumption, the standard deviation of the pixels in interferogram 6 should represent occasional changes in the backscattering due to external disturbances, such as, e.g., different meteorological conditions, or the presence of different scattering sources. Hence, the standard deviation in 6 can be assumed as representative for the "noise" of the computed differential phase measurements. From this standard deviation, it is possible to derive the standard deviation for another interferogram, say interferogram i, by a simple error propagation, rescaling for the perpendicular baseline components

$$\sigma(\delta\phi(i)) = \sigma(\delta\phi(6))\sqrt{\frac{B_\perp^2(7)+B_\perp^2(i)}{B_\perp^2(7)+B_\perp^2(6)}} \qquad (5)$$

where $\sigma(\delta\phi(i))$ is the standard deviation in i. We assumed that $\sigma^2(\Delta\phi_{\text{flat}})$ is the same for the whole series. The standard deviation determined by means of (5) from the empirical standard deviation in interferogram 6 is represented as a function of the perpendicular baseline in Fig. 4 (continuous line). The "theoretical" values derived from the value in 6, are in three cases lower than the standard deviations, as determined from the data, and in two cases higher. It is therefore impossible to draw some conclusion yet about the correctness of (5). In order to do this, a larger number of interferograms should be examined, which at the time the test was done was not possible due to the limited availability of SLC data.

VI. Summary and Conclusions

The analysis of a time series of interferograms spanning intervals from one day up to 3-1/2 yr shows that a considerable number of anthropogenic features have high coherence on long time scales. The analysis of the interferometric coherence of such features over the time series has revealed that a significant number of them also do maintain high values. In only one interferogram of the series, the coherence values decreased for all features examined. Since the effect was general, the cause for the decorrelation is likely to be systematic, such as a substantial change in the weather conditions between the time when master and slave were acquired. Indeed, the comparison of coherence for these features over the series allowed us to identify the lower quality of this interferogram. In this sense, the comparison of highly coherent sources in more interferograms could be a tool for a first assessment of the "quality" of each interferogram for INSAR applications. The analysis of anthropogenic features revealed further no significant dependence of their coherence on time.

The phase stability has been checked by applying the differential technique to a subset of the sample used for the analysis of the coherence. The subset consisted of pixels, located in an urban area, which have constant and high coherence: the area is not subject to ground deformations, so that the stability of the features with respect to any other relevant factors could be tested. The analysis showed that, at the considered level of resolution, the phase values corresponding to the highly coherent pixels seem to be in many cases stable with a standard deviation estimated from the data of the order of at least 0.5 radians. The elimination of one interferogram as a result of the coherence analysis and the selection for the phase analysis, of only those interferograms having baselines shorter than the baseline of the reference one, has limited, however, the time series to six elements. Moreover, in one of the interferograms, the differential phase values turned out to be generally corrupted, probably due to atmospheric disturbances. It is evident that the number of interferograms of our time series is a limiting factor in the assessment of the results. In this respect, we expect that the availability of a time series with a larger number of interferograms will permit us to obtain more clear results. A richer time series would make the identification of "bad" interferograms easier, and at the same time, the exclusion of such interferograms would not affect significantly the quality of the time series itself. Finally, it has to be stressed that these are the first attempts to assess whether phase information coming from very small structures, whose reflection is limited to one or few more pixels, can be used for extending the time range applicability of the INSAR technique. In this sense, the results presented are an encouragement to perform more refined tests to study the interferometric characteristics of such features.

Acknowledgment

The authors would like to thank P. Visser and R. Scharroo of DEOS for providing the ERS precise orbits.

References

[1] D. Geudtner, "The interferometric processing of ERS-1 SAR data," ESA Tech. Translation, ESA-TT-1341, Nov. 1996.

[2] D. Just and R. Bamler, "Phase statistics of interferograms with applications to synthetic aperture radar," *Appl. Opt.,* vol. 33, no. 20, pp. 4361–4368, 1994.

[3] E. Rodriguez and J. M. Martin, "Theory and design of interferometric synthetic aperture radars," in *IEE Proc.-F,* Apr. 1992, vol. 139, no. 2, pp. 147–159.

[4] M. Schwäbisch, *Die SAR-Interferometrie zur Erzeugung digitaler Geländemodelle,* Forschungsbericht 95-25, Deutsche Forschungsanstalt für Luft-und Raumfahrt (DLR), Oberpfaffenhofen, Germany, July 1995.

[5] H. A. Zebker, P. A. Rosen, R. M. Goldstein, A. Gabriel, and C. L. Werner, "On the derivation of coseismic displacement fields using differential radar interferometry: The Landers earthquake," *J. Geophys. Res.,* vol. 99, pp. 19 617–19 634, Oct. 1994.